PCCP

ARTICLE TYPE

Cite this: DOI: 00.0000/xxxxxxxxxx

A quantitative analysis of two-fold electrical conductivity relaxation behaviour in mixed proton–oxide-ion–electron conductors upon hydration

Andreas Falkenstein,*[a,b] Roger A. De Souza,[a,b] Wilhelm A. Meulenberg,[b,c,d] and Manfred Martin[a,b]

Received Date
Accepted Date

DOI: 00.0000/xxxxxxxxxx

Electrical conductivity relaxation experiments on oxides with three mobile charge carriers, H^+, O^{2-} and e^-, yield in (de-)hydration experiments up to four kinetic parameters (diffusion coefficients and surface reaction constants). In addition, three amplitude factors are obtained, but they have not been given further consideration because quantitative expressions for their forms are lacking. In this study, the forms of the amplitude factors are derived based on a simple kinetic approach and exact definitions for a diffusion-limited and a surface-reaction-limited case are given. In order to demonstrate the benefits of the approach, the electrical conductivity relaxation behaviour of lanthanum tungstate ($La_{5.4}WO_{11.1-0.2\delta}$, LaWO54) was investigated experimentally over the temperature range $923 \leq T/K \leq 1223$. A switch from two-fold non-monotonic relaxation behaviour at high temperatures to a two-fold monotonic behaviour at low temperatures upon hydration was observed. The switch in signs of the fast kinetics' amplitude factor can be assigned to the electrochemical mobility of protons surpassing the electron-hole mobility with decreasing temperature.

1 Introduction

The electrical conductivity relaxation (ECR) technique is widely used to determine the oxygen transport parameters of mixed ionic-electronic conducting materials. The two charge carriers considered are oxygen vacancies or interstitials and electronic defects. In mixed conductors with two types of ionic charge carriers (oxide ions and protons) and electronic defects, the description of transport kinetics is more complicated. Yoo et al.[1,2] extended the ECR technique and determined the transport parameters of hydrogen and oxygen in one measurement by using a step-like change in partial pressure of water, ΔpH_2O, whilst maintaining a constant partial pressure of oxygen, i.e. for hydrating and dehydrating steps.

The observed two-fold relaxation curve can be described with a superposition of two single-fold relaxation curves, $f_H(t)$ and $f_O(t)$, with amplitude factors for the initial conductivity ($\tilde{A}$) and for each curve ($\tilde{B}$ and $\tilde{C}$):

$$\sigma(t) = \tilde{A} + \tilde{B} \cdot f_H(t) + \tilde{C} \cdot f_O(t) \quad (1)$$

According to Yoo et al., the amplitude factors are functions of initial and final concentrations and electrochemical mobilities.[1] The exact forms of the amplitude factors have been ignored until now, however, on account of their complexity. If the relaxation is not only diffusion-controlled[1,3], but also limited by surface reactions, the shape function of the diffusion model with diffusion-limitation can be replaced by the function of the model giving also respect to the surface reaction.[4,5] The corresponding analyt-

[a] RWTH Aachen University, Institute of Physical Chemistry, Landoltweg 2, Aachen, Germany. Fax: +49 241 80 92128; Tel: +49 241 80 94757; E-mail: falkenstein@pc.rwth-aachen.de
[b] JARA-Energy, Germany.
[c] Forschungszentrum Jülich GmbH, Institut für Energie- und Klimaforschung IEK-1: Werkstoffsynthese und Herstellungsverfahren, Leo-Brandt-Str., Jülich, Germany.
[d] University of Twente, Faculty of Science and Technology, P.O Box 217, Enschede, Netherlands.
† Electronic Supplementary Information (ESI) available. See DOI: 10.1039/cXCP00000x/

ical solution can be found in the appendix.[6]

In this study we derive the amplitude factors for the diffusion-limited and for the surface-reaction-limited case. In addition, ECR experiments were performed on a material for which we expect significant changes in the amplitude factors, i.e. a material with two ionic mobile charge carriers together with electronic charge carriers, and a large change in protonic and electronic contribution to the conductivity. $La_{5.4}WO_{11.1\text{-}0.2\delta}$ (LaWO54) is such a material. Previously, Solis et al.[7] performed hydration experiments and found at low temperature (negligible electronic conductivity) single-fold relaxation behaviour. In contrast, Ruf et al.[8] examined Mo-doped Neodymium tungstate and observed two-fold non-monotonic behaviour, on account of high electronic conductivity. In this study we aim to observe both in one system, and this can be achieved by investigating LaWO54 at low and high temperatures.

1.1 Structure and Defect Chemistry of Lanthanum Tungstate

Lanthanum tungstate has been identified as a good protonic conductor with high chemical and mechanical stability.[9–13] The general chemical formula of fluorite-type lanthanum tungstates can be written as $La_{28-x}W_{4+x}O_{54+1.5x}v_{2-1.5x}$. With increasing x, structural oxygen vacancies $v_v^\times$ are filled with oxygen ions to compensate the excess tungsten ($W_{La}^{\bullet\bullet\bullet}$), leading to an effective negatively charged oxygen on a structural oxygen vacancy site, O_v''. Here, we only consider $x = 1$ which gives a reduced chemical formula of $La_{5.4}WO_{11.1-0.2\delta}$.[14–17] The defect chemistry of LaWO54 can be described by two perspectives. Erdal et al. described the first perspective by inherently defective sublattices with fractional charges.[18,19] They also stated that some vacancies neighboring tungsten are only slightly higher in energy and for high temperatures, all oxygen sites can be assumed degenerate. The second perspective consists of an order/disorder transition such as that observed for spinels[20]. Accordingly, the oxygen species and the vacancy species of regular oxygen sites and structural vacancies are in a fixed relation for degenerate lattices. Although excess tungsten in LaWO54 is an electron donor, it shows – in combination with occupied structural vacancies – the behaviour of an acceptor-doped p-type mixed conductor with $[Acc']_{eff} \approx 1$.[17] Here, we only consider the latter perspective as it is sufficient to describe the transport properties. The electroneutrality condition of LaWO54 with $2[O_v''] - 3[W_{La}^{\bullet\bullet\bullet}] = [Acc']_{eff}$ is hence under oxidizing conditions and considering also protons

$$[h^\bullet] + 2[v_O^{\bullet\bullet}] + [H_i^\bullet] = [Acc']_{eff} \tag{2}$$

In ceramic oxides, protons are bound to oxygen ions forming free hydroxide-anions, $OH_O^\bullet$ (compare to the perovskite type oxides discussed in References[21–23]). They can also be described in defect-chemical terms as proton interstitials, $H_i^\bullet$.[24] The oxygen and hydrogen species in the bulk phase are in equilibrium with their component chemical activities in the surrounding gas phase and can be incorporated or released by surface reactions. The thermodynamics of this system can be specified with two partial pressures, pH_2O and pO_2. For water vapor, the insertion reaction can be formulated as

$$H_2O(g) + v_O^{\bullet\bullet} + O_O^\times \rightleftharpoons 2OH_O^\bullet \left(\equiv 2O_O^\times + 2H_i^\bullet\right) \tag{3}$$

Under oxidizing conditions and in the presence of electron holes, the water insertion reaction can be divided into a hydrogen insertion reaction and an oxygen insertion reaction, each with their own insertion kinetics:

$$2\times \qquad \frac{1}{2}H_2(g) + h^\bullet \rightleftharpoons H_i^\bullet \tag{4}$$

$$1\times \qquad \frac{1}{2}O_2(g) + v_O^{\bullet\bullet} \rightleftharpoons O_O^\times + 2h^\bullet \tag{5}$$

2 Theory: Amplitude Factors

The amplitude factors in Eq. (1) will first be discussed for a simple, phenomenological approach followed by the derivation of the amplitude factors with a general description for a diffusion-limited or a surface-reaction-limited case. Finally, a combination of both cases will be discussed.

2.1 Simple Approach

For a first, simple approach, we consider thin samples with the sample's half-thickness a, for which the relaxation is limited by the surface reaction only. The analytical solution is hence a simple exponential function, and for three mobile charge carriers, the relaxation is a superposition of two simple exponential functions. The oxygen concentration that is in equilibrium with the surrounding gas atmosphere is a time-dependent concentration because the proton interstitial concentration changes with time. In the simple approach, however, we assume that both hydration-reactions described in Eqs. (4) and (5) are forward-reactions only and that the incorporation of hydrogen is faster than the incorporation of oxygen. Thus, the time dependent oxygen vacancy concentration is

$$c_v(t) = c_v^0 + (c_v^{eq} - c_v^0) \cdot \left(1 - e^{-\frac{k_O}{a}t}\right) \tag{6}$$

and it is dependent on the reactants in Eq. (5) only. In contrast, we assume that the equilibrium concentration of hydrogen, c_H^{eq}, is a function of the oxygen vacancy concentration, linked by the electron hole concentration: the incorporation of oxygen increases the electron hole concentration and the hydrogen inser-

tion reaction, Eq. (4), is hence shifted farther to the right hand side. Eq. (6) can be inserted into the equilibrium hydrogen concentration in the flux equation for proton interstitials:

$$j_{\mathrm{H}} = \tilde{k}_{\mathrm{H}} \left\{ c_{\mathrm{H}}^{\mathrm{eq}} [c_{\mathrm{v}}(t)] - c_{\mathrm{H}}(t) \right\} \tag{7}$$

$$= \tilde{k}_{\mathrm{H}} \left\{ c_{\mathrm{H}}^{\mathrm{eq}}(c_{\mathrm{v}}^{0}) + \left[c_{\mathrm{H}}^{\mathrm{eq}} - c_{\mathrm{H}}^{\mathrm{eq}}(c_{\mathrm{v}}^{0}) \right] \cdot \left(1 - e^{-\frac{\tilde{k}_{\mathrm{O}}}{a} t} \right) - c_{\mathrm{H}}(t) \right\}$$

Here, the concentration $c_{\mathrm{H}}^{\mathrm{eq}}$ is the final hydrogen concentration, c_{H}^{0} the initial hydrogen concentration, and $c_{\mathrm{H}}^{\mathrm{eq}}(c_{\mathrm{v}}^{0})$ the final concentration of hydrogen that would be in equilibrium with the initial vacancy concentration (e.g. either deep within the sample or if the mobility of oxygen vacancies would be zero). The time-dependent concentration of hydrogen is

$$c_{\mathrm{H}}(t) = c_{\mathrm{H}}^{0} + \left[c_{\mathrm{H}}^{\mathrm{eq}} - c_{\mathrm{H}}^{0} - \frac{c_{\mathrm{H}}^{\mathrm{eq}} - c_{\mathrm{H}}^{\mathrm{eq}}(c_{\mathrm{v}}^{0})}{1 - \frac{\tilde{k}_{\mathrm{O}}}{\tilde{k}_{\mathrm{H}}}} \right] \left(1 - e^{-\frac{\tilde{k}_{\mathrm{H}}}{a} t} \right) \tag{8}$$

$$+ \frac{c_{\mathrm{H}}^{\mathrm{eq}} - c_{\mathrm{H}}^{\mathrm{eq}}(c_{\mathrm{v}}^{0})}{1 - \frac{\tilde{k}_{\mathrm{O}}}{\tilde{k}_{\mathrm{H}}}} \left(1 - e^{-\frac{\tilde{k}_{\mathrm{O}}}{a} t} \right)$$

The total conductivity is the sum of the conductivities of all charge carriers, $\sigma = F \sum_i (|z_i| u_i c_i)$. Assuming constant mobilities u_i and fast hydrogen kinetics, $1 \gg \tilde{k}_{\mathrm{O}} / \tilde{k}_{\mathrm{H}}$, the total conductivity is hence a superposition of two simple exponential functions and a time-dependent change in electron hole concentration:

$$\sigma(t) = A + B \left(1 - e^{-\frac{\tilde{k}_{\mathrm{H}}}{a} t} \right) + C \left(1 - e^{-\frac{\tilde{k}_{\mathrm{O}}}{a} t} \right) + E c_{\mathrm{h}^{\bullet}}(t) \tag{9}$$

with

$$A = F \left(|z_{\mathrm{H}}| u_{\mathrm{H}} c_{\mathrm{H}}^{0} + |z_{\mathrm{v}}| u_{\mathrm{v}} c_{\mathrm{v}}^{0} \right)$$

$$B = F |z_{\mathrm{H}}| u_{\mathrm{H}} \left[c_{\mathrm{H}}^{\mathrm{eq}}(c_{\mathrm{v}}^{0}) - c_{\mathrm{H}}^{0} \right]$$

$$C = F |z_{\mathrm{v}}| u_{\mathrm{v}} (c_{\mathrm{v}}^{\mathrm{eq}} - c_{\mathrm{v}}^{0}) + F |z_{\mathrm{H}}| u_{\mathrm{H}} \left[c_{\mathrm{H}}^{\mathrm{eq}} - c_{\mathrm{H}}^{\mathrm{eq}}(c_{\mathrm{v}}^{0}) \right]$$

$$E = F |z_{\mathrm{h}^{\bullet}}| u_{\mathrm{h}^{\bullet}}$$

The time-dependent concentration of electron holes is a function of the oxygen vacancy and hydrogen concentration due to the electroneutrality condition, Eq. (2):

$$c_{\mathrm{h}^{\bullet}}(t) = c_{\mathrm{h}^{\bullet}}^{0} - 2 \left[c_{\mathrm{v}}(t) - c_{\mathrm{v}}^{0} \right] - \left[c_{\mathrm{H}}(t) - c_{\mathrm{H}}^{0} \right] \tag{10}$$

It can be inserted into Eq. (9) and by a combination with the equations for $c_{\mathrm{v}}(t)$ and $c_{\mathrm{H}}(t)$, the final equation for the time-dependent conductivity can be obtained:

$$\sigma(t) = \tilde{A} + \tilde{B} \left(1 - e^{-\frac{\tilde{k}_{\mathrm{H}}}{a} t} \right) + \tilde{C} \left(1 - e^{-\frac{\tilde{k}_{\mathrm{O}}}{a} t} \right) \tag{11}$$

The amplitude factors are:

$$\tilde{A} = F \sum_i \left(|z_i| u_i c_i^{0} \right) \tag{12}$$

$$\tilde{B} = F \left[c_{\mathrm{H}}^{\mathrm{eq}}(c_{\mathrm{v}}^{0}) - c_{\mathrm{H}}^{0} \right] (|z_{\mathrm{H}}| u_{\mathrm{H}} - |z_{\mathrm{h}^{\bullet}}| u_{\mathrm{h}^{\bullet}}) \tag{13}$$

$$\tilde{C} = F \left[c_{\mathrm{v}}^{\mathrm{eq}} - c_{\mathrm{v}}^{0} \right] (|z_{\mathrm{v}}| u_{\mathrm{v}} - 2 |z_{\mathrm{h}^{\bullet}}| u_{\mathrm{h}^{\bullet}}) \tag{14}$$

$$+ F \left[c_{\mathrm{H}}^{\mathrm{eq}} - c_{\mathrm{H}}^{\mathrm{eq}}(c_{\mathrm{v}}^{0}) \right] (|z_{\mathrm{H}}| u_{\mathrm{H}} - |z_{\mathrm{h}^{\bullet}}| u_{\mathrm{h}^{\bullet}})$$

The downside of the simple approach is the fact that the analytical solution cannot be adapted for a model including both surface reaction and diffusion limitation, because the boundary condition linking the surface reaction with the diffusion at the surface, Eq. (30) in appendix A, does not hold. A more detailed discussion on the surface boundary condition can be found in section 2.4.

2.2 Diffusion Limitation

The flux of one species is influenced by both the gradient of its own concentration and the gradient of the concentration of the second species.[25–28] The flux of the third mobile species is dependent on the other species via the dynamic electroneutrality condition $2 j_{\mathrm{v}_{\mathrm{O}}^{\bullet\bullet}} + j_{\mathrm{H}_{\mathrm{i}}^{\bullet}} + j_{\mathrm{h}^{\bullet}} = 0$. As discussed by Poetzsch et al.[27], the flux equations for both species are

$$j_{\mathrm{H}_{\mathrm{i}}^{\bullet}} = -D_{\mathrm{HH}} \nabla c_{\mathrm{H}_{\mathrm{i}}^{\bullet}} - D_{\mathrm{Hv}} \nabla c_{\mathrm{v}_{\mathrm{O}}^{\bullet\bullet}} \tag{15}$$

$$j_{\mathrm{v}_{\mathrm{O}}^{\bullet\bullet}} = -D_{\mathrm{vH}} \nabla c_{\mathrm{H}_{\mathrm{i}}^{\bullet}} - D_{\mathrm{vv}} \nabla c_{\mathrm{v}_{\mathrm{O}}^{\bullet\bullet}} \tag{16}$$

In the above diffusion coefficient matrix, the diagonal elements D_{HH} and D_{vv} are the chemical diffusion coefficients of $\mathrm{H}_{\mathrm{i}}^{\bullet}$ and $\mathrm{v}_{\mathrm{O}}^{\bullet\bullet}$ under their own concentration gradients, while the cross-coefficients describe chemical diffusion due to the concentration gradient of the other species.[27]

The generalized version of Fick's second law can be written in vector-form as:

$$\dot{\vec{c}} = \begin{pmatrix} \dot{c}_{\mathrm{H}_{\mathrm{i}}^{\bullet}} \\ \dot{c}_{\mathrm{v}_{\mathrm{O}}^{\bullet\bullet}} \end{pmatrix} = \begin{pmatrix} D_{\mathrm{HH}} & D_{\mathrm{Hv}} \\ D_{\mathrm{vH}} & D_{\mathrm{vv}} \end{pmatrix} \begin{pmatrix} c''_{\mathrm{H}_{\mathrm{i}}^{\bullet}} \\ c''_{\mathrm{v}_{\mathrm{O}}^{\bullet\bullet}} \end{pmatrix} = \mathbf{D} \vec{c}'' \tag{17}$$

The two coupled fluxes in Eqs. (15) and (16) can be decoupled by a diagonalization of the diffusion matrix $\mathbf{D}$ in Eq. (17) (see appendix B for a detailed description of the principal axis theorem). With this method, two eigenvalues are obtained, which are the effective chemical diffusion coefficients: $\lambda_1 = \tilde{D}_{\mathrm{H}}^{\mathrm{eff}}$ and $\lambda_2 = \tilde{D}_{\mathrm{O}}^{\mathrm{eff}}$.

Additionally, decoupled concentrations $\tilde{c}_1$ and $\tilde{c}_2$ are obtained, both with contributions of protons and oxygen vacancies. The decoupled versions of Fick's second law now read

$$\dot{\tilde{c}}_1 = \lambda_1 \tilde{c}_1'' \qquad \dot{\tilde{c}}_2 = \lambda_2 \tilde{c}_2'' \tag{18}$$

The analytical solution for the diffusion limited concentration profile[6] can be used for each equation. By transforming the decoupled concentration vector back to the species' concentrations ($\vec{c} = \mathbf{S}\vec{\tilde{c}}$), see appendix B, the time-dependent concentration profiles of each species can be calculated:

$$\begin{aligned} c_{\mathrm{H_i^\bullet}}(x,t) = &- \frac{D_{\mathrm{Hv}}}{\sqrt{(D_{\mathrm{HH}} - \lambda_1)^2 + D_{\mathrm{Hv}}^2}} \cdot \tilde{c}_1(x,t,\lambda_1) \\ &- \frac{D_{\mathrm{vv}} - \lambda_2}{\sqrt{D_{\mathrm{vH}}^2 + (D_{\mathrm{vv}} - \lambda_2)^2}} \cdot \tilde{c}_2(x,t,\lambda_2) \end{aligned} \tag{19}$$

$$\begin{aligned} c_{\mathrm{v_O^{\bullet\bullet}}}(x,t) = &\left[1 + \left(\frac{D_{\mathrm{Hv}}}{D_{\mathrm{HH}} - \lambda_1}\right)^2\right]^{-1/2} \cdot \tilde{c}_1(x,t,\lambda_1) \\ &+ \left[1 + \left(\frac{D_{\mathrm{vv}} - \lambda_2}{D_{\mathrm{vH}}}\right)^2\right]^{-1/2} \cdot \tilde{c}_2(x,t,\lambda_2) \end{aligned} \tag{20}$$

By an integration of the diffusion profiles, mean values of the concentrations can be calculated, and subsequently the electrical conductivity relaxation curves can be obtained. They are also superpositions of two relaxation curves with kinetic parameters λ_1 and λ_2 (the effective diffusion coefficients). Here, also a set of amplitude factors can be calculated from Eq. (10). The factor $\tilde{A}$ remains the same as in Eq. (11) while both $\tilde{B}$ and $\tilde{C}$ now have two contributions each. The amplitude factors are defined as follows, with the corresponding elements of the matrix $\mathbf{S}$, defined in appendix B:

$$\begin{aligned} \tilde{B} = &F\left(|z_{\mathrm{H_i^\bullet}}|u_{\mathrm{H_i^\bullet}} - |z_{\mathrm{h^\bullet}}|u_{\mathrm{h^\bullet}}\right) S_{11}\left(\tilde{c}_1^{\mathrm{eq}} - \tilde{c}_1^0\right) \\ &+ F\left(|z_{\mathrm{v_O^{\bullet\bullet}}}|u_{\mathrm{v_O^{\bullet\bullet}}} - 2|z_{\mathrm{h^\bullet}}|u_{\mathrm{h^\bullet}}\right) S_{21}\left(\tilde{c}_1^{\mathrm{eq}} - \tilde{c}_1^0\right) \end{aligned} \tag{21}$$

$$\begin{aligned} \tilde{C} = &F\left(|z_{\mathrm{H_i^\bullet}}|u_{\mathrm{H_i^\bullet}} - |z_{\mathrm{h^\bullet}}|u_{\mathrm{h^\bullet}}\right) S_{12}\left(\tilde{c}_2^{\mathrm{eq}} - \tilde{c}_2^0\right) \\ &+ F\left(|z_{\mathrm{v_O^{\bullet\bullet}}}|u_{\mathrm{v_O^{\bullet\bullet}}} - 2|z_{\mathrm{h^\bullet}}|u_{\mathrm{h^\bullet}}\right) S_{22}\left(\tilde{c}_2^{\mathrm{eq}} - \tilde{c}_2^0\right) \end{aligned} \tag{22}$$

2.3 Surface Reaction Limitation

A more detailed derivation of the amplitude factors for a surface reaction limited case with exemplary rate determining steps for the incorporation of water into the bulk phase is done in this section. The following steps for the incorporation of water are assumed to be in pre-equilibrium: a water molecule from the gas phase is adsorbed at the surface and dissociates into adsorbed hydrogen and oxygen atoms. We assume furthermore that one rate determining step is the transfer of an electron hole to the adsorbed hydrogen atom, incorporating a proton interstitial:

$$\mathrm{H_{ad} + h^\bullet} \underset{\overleftarrow{k}_{\mathrm{H}}}{\overset{\overrightarrow{k}_{\mathrm{H}}}{\rightleftharpoons}} \mathrm{H_i^\bullet} \qquad \text{with} \qquad K_{\mathrm{H}} = \frac{\overrightarrow{k}_{\mathrm{H}}}{\overleftarrow{k}_{\mathrm{H}}} = \frac{[\mathrm{H_i^\bullet}]^{\mathrm{eq}}}{[\mathrm{H_{ad}}]^{\mathrm{eq}}[\mathrm{h^\bullet}]^{\mathrm{eq}}} \tag{23}$$

For oxygen, two electron holes must be transferred of which the second electron hole transfer is assumed to be rate determining:

$$\mathrm{O_{ad}^- + v_O^{\bullet\bullet}} \underset{\overleftarrow{k}_{\mathrm{O}}}{\overset{\overrightarrow{k}_{\mathrm{O}}}{\rightleftharpoons}} \mathrm{O_O^\times + h^\bullet} \quad \text{with} \quad K_{\mathrm{O}} = \frac{\overrightarrow{k}_{\mathrm{O}}}{\overleftarrow{k}_{\mathrm{O}}} = \frac{[\mathrm{O_O^\times}]^{\mathrm{eq}}[\mathrm{h^\bullet}]^{\mathrm{eq}}}{[\mathrm{O_{ad}^-}]^{\mathrm{eq}}[\mathrm{v_O^{\bullet\bullet}}]^{\mathrm{eq}}} \tag{24}$$

Upon a small change in $p\mathrm{H_2O}$, the defect fractions involved in the rate determining step are changed by a small amount x for Eq. (23) and y for Eq. (24) with first order reactions. The new time dependent concentrations are

$$\begin{aligned} [\mathrm{H_{ad}}](t) &= [\mathrm{H_{ad}}]^{\mathrm{eq}} - x(t) & [\mathrm{H_i^\bullet}](t) &= [\mathrm{H_i^\bullet}]^{\mathrm{eq}} + x(t) \\ [\mathrm{O_{ad}^-}](t) &= [\mathrm{O_{ad}^-}]^{\mathrm{eq}} - y(t) & [\mathrm{O_O^\times}](t) &= [\mathrm{O_O^\times}]^{\mathrm{eq}} + y(t) \\ [\mathrm{v_O^{\bullet\bullet}}](t) &= [\mathrm{v_O^{\bullet\bullet}}]^{\mathrm{eq}} - y(t) & [\mathrm{h^\bullet}](t) &= [\mathrm{h^\bullet}]^{\mathrm{eq}} - x(t) + y(t) \end{aligned} \tag{25}$$

The change of the amounts x and y with respect to time are the changes of hydrogen and oxygen concentrations, respectively, and can be expressed as

$$\frac{dx}{dt} = \overrightarrow{k}_{\mathrm{H}}\left([\mathrm{H_{ad}}]^{\mathrm{eq}} - x\right)\left([\mathrm{h^\bullet}]^{\mathrm{eq}} - x + y\right) - \overleftarrow{k}_{\mathrm{H}}\left([\mathrm{H_i^\bullet}]^{\mathrm{eq}} + x\right) \tag{26}$$

$$\frac{dy}{dt} = \overrightarrow{k}_{\mathrm{O}}\left([\mathrm{O_{ad}^-}]^{\mathrm{eq}} - y\right)\left([\mathrm{v_O^{\bullet\bullet}}]^{\mathrm{eq}} - y\right) - \overleftarrow{k}_{\mathrm{O}}\left([\mathrm{O_O^\times}]^{\mathrm{eq}} + y\right)\left([\mathrm{h^\bullet}]^{\mathrm{eq}} - x + y\right) \tag{27}$$

From these equations, the linear dependent terms can be expressed with a matrix $\mathbf{K}$:

$$\begin{pmatrix} \dot{x} \\ \dot{y} \end{pmatrix} = \begin{pmatrix} k_{\mathrm{H}x} & k_{\mathrm{H}y} \\ k_{\mathrm{O}x} & k_{\mathrm{O}y} \end{pmatrix} \begin{pmatrix} x \\ y \end{pmatrix} \tag{28}$$

with

$$\begin{aligned} k_{\mathrm{H}x} &= -\overrightarrow{k}_{\mathrm{H}}\left([\mathrm{h^\bullet}]^{\mathrm{eq}} + [\mathrm{H_{ad}}]^{\mathrm{eq}}\right) - \overleftarrow{k}_{\mathrm{H}} \\ k_{\mathrm{H}y} &= \overrightarrow{k}_{\mathrm{H}}\,[\mathrm{H_{ad}}]^{\mathrm{eq}} \\ k_{\mathrm{O}x} &= \overleftarrow{k}_{\mathrm{O}}\,[\mathrm{O_O^\times}]^{\mathrm{eq}} \\ k_{\mathrm{O}y} &= -\overrightarrow{k}_{\mathrm{O}}\left([\mathrm{O_{ad}^-}]^{\mathrm{eq}} + [\mathrm{v_O^{\bullet\bullet}}]^{\mathrm{eq}}\right) - \overleftarrow{k}_{\mathrm{O}}\left([\mathrm{O_O^\times}]^{\mathrm{eq}} + [\mathrm{h^\bullet}]^{\mathrm{eq}}\right) \end{aligned}$$

The above equations show that in a system with three charge carriers involved, the surface reaction must be described by a (2×2) matrix of surface reaction constants. This matrix can be diagonalized in the same way as the diffusion matrix in the previous section. By integration, two simple exponential functions are obtained with the eigenvalues as effective surface reaction constants, ρ_1 and ρ_2. The concentration changes of hydrogen and oxygen are both dependent on both surface reaction constants. This exemplary derivation for two assumed rate determining steps can be adapted if experimental results suggest other rate determining steps. It is required, however, that i) two separate reactions for the incorporation of oxygen and hydrogen have to be formulated, ii) that all other reactions are in pre-equilibrium and iii) linear kinetics can be assumed by choosing small step-sizes for the changes in water and/or oxygen activities.

2.4 Diffusion and Surface Reaction Limitation

In the previous sections, the exact solutions for a diffusion-limited and a surface-reaction-limited case have been established. The commonly used analytical solution for relaxation dependent on both kinetics [Eq. (31) in the appendix] contains, however, the surface boundary condition, Eq. (30), linking the diffusion flux at the surface and the flux caused by the surface reaction. Unfortunately, the aforementioned diagonalized concentrations are not equal itself, i.e. the matrices **K** and **D** cannot be diagonalized simultaneously.

$$\begin{pmatrix} j_\mathrm{H} \\ j_\mathrm{v} \end{pmatrix}_{\text{surface}} = -\mathbf{D}\begin{pmatrix} \nabla c_\mathrm{H} \\ \nabla c_\mathrm{v} \end{pmatrix}_{\text{surface}} = \mathbf{K}\begin{pmatrix} \Delta c_\mathrm{H} \\ \Delta c_\mathrm{v} \end{pmatrix} \qquad (29)$$

with Δc_i as the driving force for the surface reaction of species i dependent on the rate determining step, e.g. the difference between surface-near concentration in the bulk and the concentration that would be in equilibrium with the surface coverage of the adsorbed species in the above example. The time-dependent concentrations of all other species (here especially oxygen vacancies) have to be considered for the equilibrium-concentration of the surface coverage. This results in a time-dependent equilibrium concentration (see simple approach). Hence, the validity of the superposition of the relaxation curves dependent on both kinetics cannot be derived because of the surface boundary condition. However, the amount of hydrogen reacting at the surface must be equal to the amount of hydrogen diffusing at the surface (or oxygen, respectively).

3 Experimental

The experimental setup is based on two different gas streams with defined oxygen and water partial pressures directed into the sample chamber via a four way valve. The flow rate and mixture of nitrogen and oxygen (5.0 purity, Westfalen AG, Germany) is adjusted by two sets of mass flow controllers (MKS Instruments, Germany). Each mixture is oversaturated in a first water vapor saturator (Quarz Glas Heinrich GmbH, Germany) and set to the desired $p\mathrm{H_2O}$ in a second water vapor saturator by directing the gas stream into a heated/cooled reservoir of water over a frit filter. One of the two gas streams with a constant $p\mathrm{O_2}$ and $p\mathrm{H_2O}$ is directed into the reaction tube over a four way valve (VICI A 90, Valco Instruments Co. Inc., USA with magnetic valve 5420, Buerkert Fluid Control Systems, Germany), which allows for very short switching times. The gas lines for humid atmospheres are heated to prevent condensation. The reactor tube resides within a furnace with a DC power supply unit (PS8160-04T, Elektro Automatik GmbH & Co. KG, Germany) to avoid influence of the commonly used pulsed heating current on the measurement.

The LaWO54 sample is a cuboid ingot with dimension $(3.69\times4.13\times33.2)$ mm^3. It was prepared by the solid state route described in References[29,30]. The sample is contacted with gold wires and paste for four-point DC measurements (2701, Keithley Instruments Inc., USA). The outer contacts provide a constant current of $20\leq I/\mu\mathrm{A}\leq500$ to the sample (2611B, Keithley Instruments Inc., USA). The potential difference is measured between the two inner contacts, placed 13 mm apart. Directly downstream of the sample a potentiometric oxygen sensor (SIRO2 C700, Ceramic Oxide Fabricators Pty. Ltd., Australia) probes the oxygen partial pressure. The oxygen flow rates have been set to show minimal difference at the potentiometric oxygen sensor between both streams. The temperature is measured by a type S thermocouple at the oxygen sensor with a distance to the sample of approximately 5 mm.

4 Results

4.1 Conductivity Relaxation upon Hydration

First experiments were performed at high temperatures (1223 K) where lanthanum tungstate shows predominant electronic conductivity[30,31] arising from electron holes. The conductivity relaxation curve of a hydrating step is shown in Fig. 1 (teal). The temperature (black) and $p\mathrm{O_2}$ (grey) remain constant throughout the experiment. The relaxation curve shows two-fold non-monotonic behaviour: after a step-like increase in $p\mathrm{H_2O}$ the conductivity rapidly drops to a minimum at a relaxation time of 37 s and then increases with slower kinetics until it reaches a constant conductivity. Following previous studies[1,4,31], we attribute the fast kinetics to the incorporation of hydrogen and the slow kinetics to the incorporation of oxygen. The initial decrease in conductivity is caused by protons incorporated into the sample at the expense of highly mobile electron holes according to Eq. (4). Afterwards, the conductivity slowly increases caused by oxygen incorporation

into the sample creating electron holes, Eq. (5). In this case, the final conductivity is higher than the initial conductivity which is not necessarily the case.

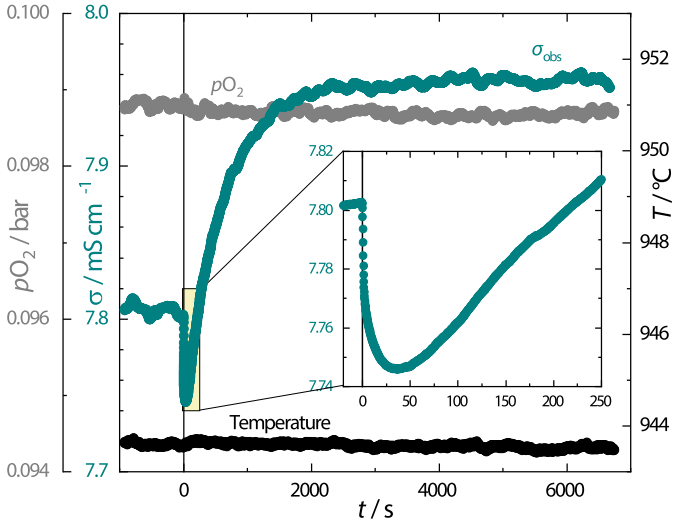

Fig. 1 Experimental conductivity relaxation curve (teal) upon hydration obtained for a LaWO54 ceramic. T = 1223 K (black); pO_2 = 200 mbar (grey); ΔpH_2O = 20 mbar (10 mbar → 30 mbar).

In order to obtain as much information as possible from a single measurement, the diffusion model giving respect to diffusion and surface reaction (see appendix A and section 2.4) has been chosen. This model can be fitted to the resulting relaxation curve by a superposition of two single-fold relaxation curves yielding the effective chemical surface reaction constants for the fast and slow kinetics, $\tilde{k}_{\mathrm{H}}^{\mathrm{eff}}$ and $\tilde{k}_{\mathrm{O}}^{\mathrm{eff}}$, respectively, and the effective chemical diffusion coefficients of both kinetics, $\tilde{D}_{\mathrm{H}}^{\mathrm{eff}}$ and $\tilde{D}_{\mathrm{O}}^{\mathrm{eff}}$.[1,5] The analytical solution for diffusion in a plane sheet with surface evaporation for two dimensions has been used.[5,6,32,33] The relaxation curve (teal) with fit is shown in Fig. 2: the superposition of the fast hydrogen kinetics (red dotted line) and of the slow oxygen kinetics (blue dotted line) with initial conductivity σ^0 as offset (black dotted line) is shown in orange. The residual of the fit is shown in the bottom panel (grey) and shows a good quality of fit with no systematic errors. Fits with less parameters (constraints $\tilde{k}_{\mathrm{H}}^{\mathrm{eff}} = \tilde{k}_{\mathrm{O}}^{\mathrm{eff}}$ or $\tilde{D}_{\mathrm{H}}^{\mathrm{eff}} = \tilde{D}_{\mathrm{O}}^{\mathrm{eff}}$) or fits using models giving respect to surface reaction only or diffusion only show systematic errors, leading to the assumption that both diffusion and surface reaction, follow two different kinetics.†

The relaxation curves are independent of the flow rate. Thus, the issues caused by large stoichiometry deviations described in Reference[34] do not affect the transport parameters, here. The relaxation behaviour upon dehydration has also been investigated. The obtained transport parameters are comparable because of the small step-size in pH_2O.

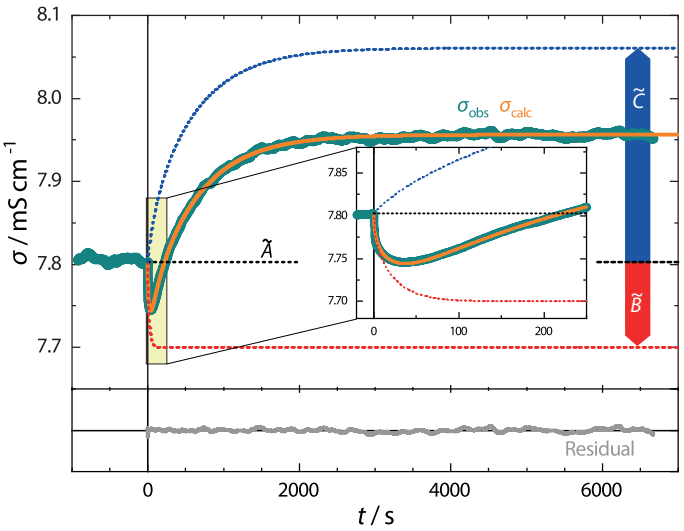

Fig. 2 ECR curve (teal) with fitted diffusion model: two single-fold relaxation curves, fast hydrogen kinetics (red dots) and slow oxygen kinetics (blue dots), and the resulting superposition (orange) with the initial conductivity as offset (black dots). Bottom panel: residual of the fit with equal scale.

4.2 Simultaneous Determinability

For single-fold relaxation curves, both parameters, $\tilde{k}$ and $\tilde{D}$, can only be determined simultaneously in one measurement if their ratio matches the sample dimension, $-0.5 < \log_{10} L_a < 2$, with $L_a = a \cdot \tilde{k}/\tilde{D}$ and the sample's half-thickness, $a \approx 0.2$ cm.[34] For two-fold curves upon hydration, two parameters, $L_{a,\mathrm{H}}$ and $L_{a,\mathrm{O}}$, can be formulated. If $L_{a,\mathrm{H}}$ and $L_{a,\mathrm{O}}$ are within the curved region in Fig. 3, all four transport parameters can be determined simultaneously. The distance between $L_{a,\mathrm{H}}$ and $L_{a,\mathrm{O}}$ in the logarithmic plot is a material property. However, both values can be shifted left or right by decreasing or increasing the sample's thickness, respectively. Thus, at least three parameters can be determined simultaneously if one adjusts the sample's thickness. The blue and red line in Fig. 3 show the parameter $L_{a,\mathrm{O}}$ and $L_{a,\mathrm{H}}$, respectively, for the fit that was performed in Fig. 2. While the parameter $L_{a,\mathrm{O}}$ is within the curved region, the parameter $L_{a,\mathrm{H}}$ is at the verge to the diffusion controlled region, meaning that it can be determined but shows rather large errors because of the fit beeing less sensitive to $\tilde{k}_{\mathrm{H}}$.

4.3 Dependence on Partial Pressure of Oxygen

The same hydration experiment has been conducted whilst decreasing the constant pO_2 for each experiment in the range from $3 \leq pO_2/\mathrm{mbar} \leq 100$. The resulting transport parameters are

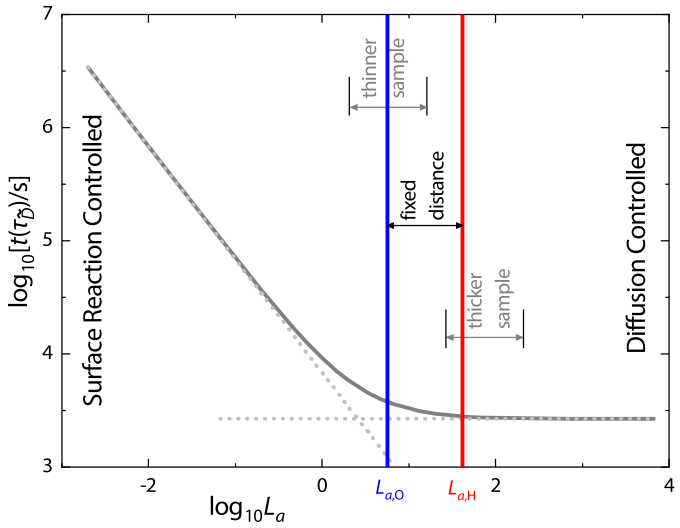

Fig. 3 Simultaneous determinability of transport parameters: in the curved region, $\tilde{k}$ and $\tilde{D}$ can be determined simultaneously. The time constant $t(\tau_{\tilde{D}})$ is the time after which approx. 97% of the relaxation progress is achieved.[34] The blue and red lines represent $L_{a,O}$ and $L_{a,H}$ for the transport parameters obtained by fitting the diffusion model to the curve shown in Fig. 2.

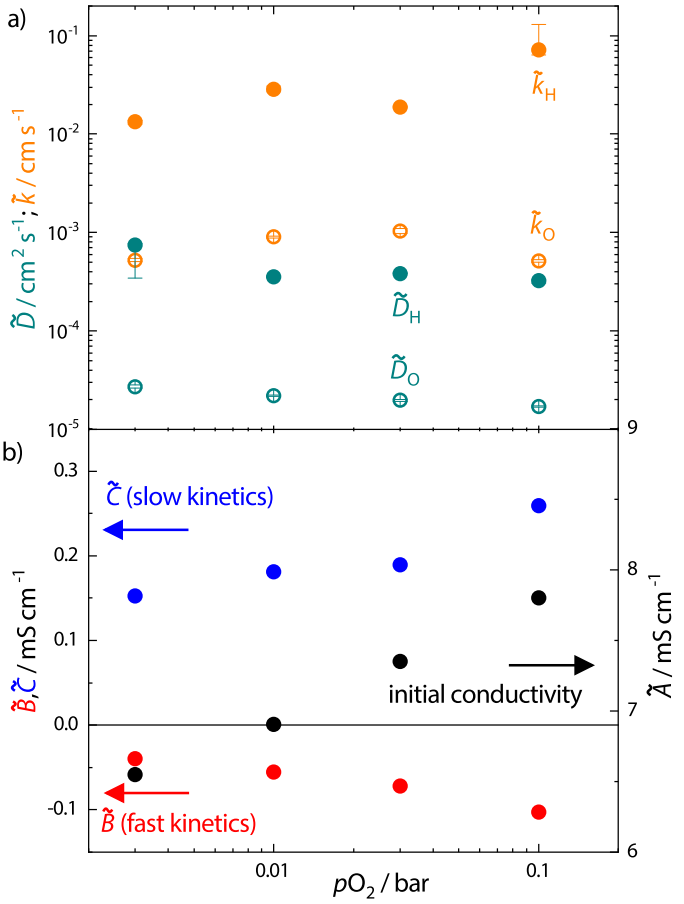

Fig. 4 a) Surface reaction constants (orange) and diffusion coefficients (teal) of the fast hydrogen kinetics (closed symbols) and slow oxygen kinetics (open symbols) upon hydration in dependence of constant pO_2. T = 1223 K, ΔpH_2O = 20 mbar (10 mbar → 30 mbar). b) Corresponding amplitude factors. Black: initial conductivity $\sigma^0 = \tilde{A}$, right scale; red: fast kinetics $\tilde{B}$; blue: slow kinetics $\tilde{C}$, both left scale.

shown in Fig. 4. They show only a weak dependence on pO_2. However, with decreasing partial pressure of oxygen, the two-fold behaviour of the relaxation curve becomes less pronounced, i.e. the drop in conductivity in the first seconds of the relaxation is smaller. The amplitude factors of the relaxation curves are shown in Figure 4. As expected, the initial conductivity increases with increasing pO_2 ($\sigma \propto pO_2^{0.05}$) suggesting electron hole conductivity. The absolute values of the amplitude factors are increasing with increasing pO_2, i.e. the two-fold relaxation characteristics are more pronounced. From the amplitude factors defined in the simple approach, Eq. (11), the increase in $|\tilde{B}|$ can be assigned to a larger difference in proton concentration upon hydration assuming constant charge and mobility. The increase in $|\tilde{C}|$ can also be attributed to a larger difference in oxygen concentration. The value of $|\tilde{C}|$ is increasing though the attenuation caused by proton incorporation, shown by the latter term in the definition of $\tilde{C}$, should also increase.

4.4 Temperature Dependence

Starting at the conditions described in Fig. 1, the relaxation experiments have been performed at various temperatures. The two-fold behaviour at high temperatures becomes less pronounced at decreasing temperatures until the relaxation became nearly single-fold for approx. 1000 K (compare to Ref.[7,31]). Single-fold behaviour is expected for hydration kinetics with negligible electronic conductivity[35]. If one further decreases the temperature, the two-fold relaxation behaviour is recurring – yet monotonic. The corresponding relaxation curve for 923 K is shown in Fig. 5. In the first few seconds, the conductivity increases with fast kinetics, followed by a further increase with slow kinetics. The quality of fit for the first few seconds is, however, not as good as for well pronounced non-monotonic curves at high temperatures. Two-fold monotonic relaxation behaviour was reported in two scenarios which do not apply here: Preis and Sitte[36] described this behaviour for materials with small grain sizes and a significant difference in bulk and grain boundary diffusivities. The grain size in this study is, however, larger (9 to 24 μm compared to 4 μm in their article). In addition, the difference in the obtained diffusivities is not as large as in the article

mentioned. In the second scenario described by Yoo and Lee,[3] the mobile species are of different kind.

The transport parameters are shown in an Arrhenius plot in

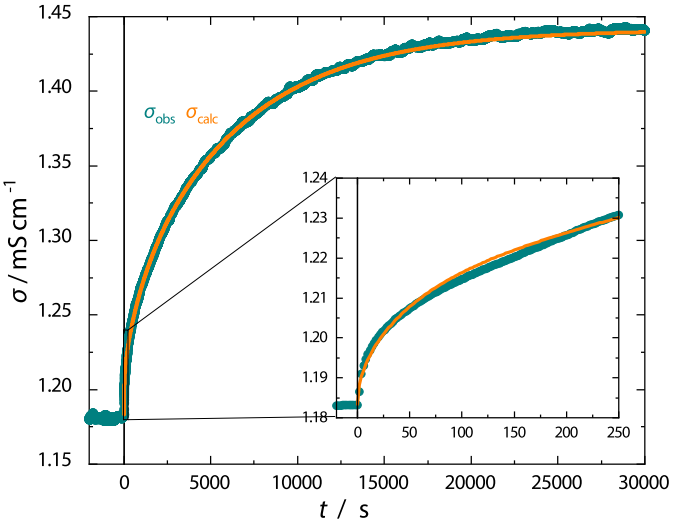

Fig. 5 Relaxation curve for low temperatures with two-fold monotonic relaxation behaviour. T = 923 K, pO_2 = 100 mbar, ΔpH_2O = 20 mbar (10 mbar → 30 mbar).

Fig. 6. For 923 K, $\tilde{k}_H$ could not be determined because the fit is independent of this parameter ($\log_{10} L_{a,H} > 2$, see Fig. 3). The parameters of the fast kinetics obtained for 973 K seem to be overestimated. The contribution of the fast kinetics to the relaxation curve is very small and the fit is thus not very sensitive to these parameters. From the Arrhenius plot, the following activation energies have been determined: $E_A(\tilde{k}_H) = 2.28(22)$ eV; $E_A(\tilde{k}_O) = 0.67(2)$ eV; $E_A(\tilde{D}_H) = 0.49(7)$ eV; $E_A(\tilde{D}_O) = 0.86(12)$ eV. The activation energies of the oxygen kinetics are in agreement with literature.[7]

The amplitude factors of the temperature dependent relaxations are shown in Fig. 6 b). The initial conductivity, $\sigma^0 = \tilde{A}$, decreases approximately linear in the Arrhenius plot for the temperature region examined in this work. The amplitude factor of the slow oxygen kinetics, $\tilde{C}$, shows no clear trend. It is always positive for hydrating steps between 0.2 and 0.3 mS cm^{-1}. The amplitude factor of the fast hydrogen kinetics $\tilde{B}$, on the other hand, has a diminished absolute value for lower temperatures as it is first expected. However, it switches sign between 973 K and 1023 K. Thus, at or above 1023 K, two-fold non-monotonic relaxation behaviour can be observed — the amplitude factors $\tilde{B}$ and $\tilde{C}$ have different signs. At or below 973 K, two-fold monotonic relaxation behaviour can be observed — both amplitude factors have the same sign. Between these temperatures, the relaxation is single-fold. Therefore, a third mobile charge carrier must be

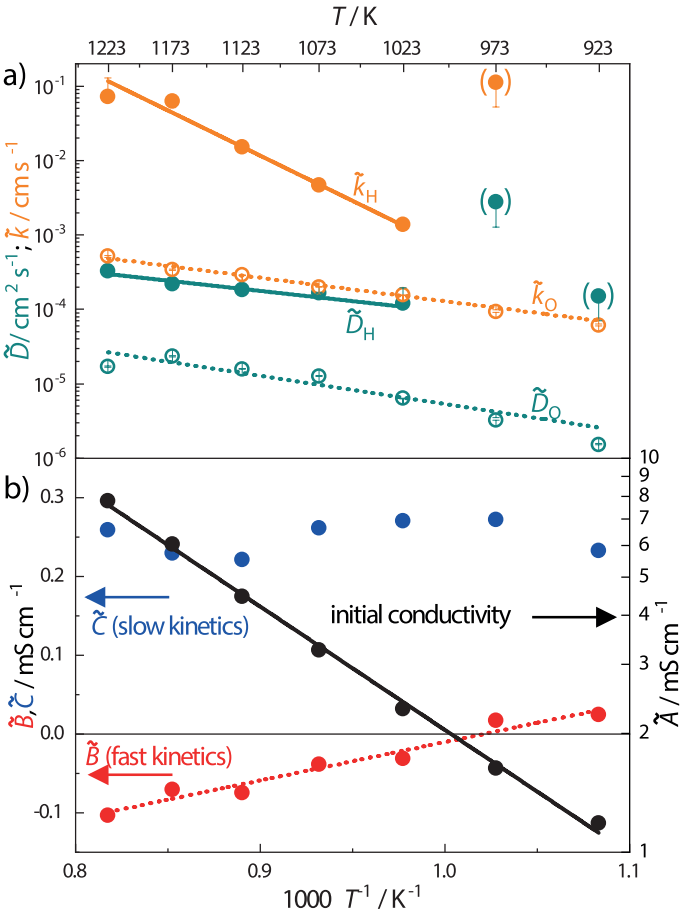

Fig. 6 Temperature dependence of parameters obtained from ECR measurements for pO_2 = 100 mbar, ΔpH_2O = 20 mbar (10 mbar → 30 mbar). a) Surface reaction constants (orange) and diffusion coefficients (teal) for hydrogen (closed symbols) and for oxygen (open symbols). b) Corresponding amplitude factors. Black: initial conductivity $\sigma^0 = \tilde{A}$, right scale; red: fast kinetics $\tilde{B}$; blue: slow kinetics $\tilde{C}$, both left scale. The red dotted line is a guide to the eye.

present, i.e. electron holes enable the splitting of the water incorporation reaction.

With the simple, phenomenological definition of the amplitude factor $\tilde{B}$, see Eq. (11), the experimentally observed switch of signs can be attributed to a specific chemical property: for hydrating steps, the change in hydrogen concentration is always positive. For temperatures at or above 1023 K, the second term must hence be negative. Proton interstitials and electron holes have a constant charge of +1 and the charge does not change with ΔpH_2O. Therefore, the electrochemical mobility of electron holes must be larger than the electrochemical mobility of proton interstitials. For temperatures at or below 973 K, the mobility of proton interstitials must be larger than the mobility of electron holes in order

to render $\tilde{B}$ positive. For a temperature between 973 K and 1023 K, where $u_H = u_{h^\bullet}$, the relaxation becomes single-fold ($\tilde{B} = 0$), although the concentration of hydrogen changes with the fast kinetics. However, this effect cannot be observed by monitoring the total electrical conductivity.

The switch in signs of $\tilde{B}$ can also be explained by the exact definitions in the diffusion-limited case when a similar assumption like in the simple approach is introduced: the flux of oxygen vacancies caused by a gradient of proton interstitials is negligible ($D_{vH} \ll D_{vv}$ if $t_v \ll 1$, see Ref.[27]). This is represented by the orthogonal matrix's element S_{22} being approximately unity and the prefactor of the second term in Eq. (20) being negligible, $S_{21} \approx 0$. The oxygen concentration profile is thus independent of $\tilde{c}_1$. Both other elements, S_{11} and S_{12}, are usually not near 0 or 1 which means that the diffusion of hydrogen is dependent on the gradient of proton interstitials and oxygen vacancies. The same explanation for the switch in signs of $\tilde{B}$ is expressed in Eq. (21): the electrochemical mobility of proton interstitials must exceed the electronic mobility in order to $\tilde{B}$ being positive upon hydration.

For the sake of completeness, there are also two other scenarios which would result in single-fold ECR behaviour upon hydration: The first covers equal diffusion coefficients and surface reaction constants for both species, $\tilde{D}_H^{eff} = \tilde{D}_O^{eff}$ and $\tilde{k}_H^{eff} = \tilde{k}_O^{eff}$. In this scenario, the shape functions are equal and a combined amplitude factor ($\tilde{B} + \tilde{C}$) is experimentally accessible. The second scenario is a negligible electronic contribution to the conductivity, i.e. the flux of oxygen vacancies is compensated by a flux of protons, with a chemical diffusion coefficient of water, D_{H_2O} (see Reference[37]).

5 Concluding Remarks

The amplitude factors that are obtained when evaluating two-fold ECR curves upon hydration have been derived for a simple, phenomenological approach and exact definitions for a diffusion-limited case and for a surface-reaction-limited are given. It is shown that not only for the diffusion[27] but also for the surface reaction four different reaction constants can be defined in a system with three mobile charge carriers that are involved in the reaction. By a diagonalization of the flux- or surface-reaction-matrix, two effective diffusion coefficients or two effective surface reaction constants are obtained, respectively. The simultaneous diagonalization for a case where the relaxation is dependent on both kinetics, however, is not possible as the diagonalized concentrations are not equal.

The ECR behaviour of proton conducting lanthanum tungstate upon hydration was investigated. The shape of the ECR curve upon hydration changes with temperature in LaWO54: from two-fold monotonic via single-fold to two-fold non-monotonic relaxation behaviour at high temperatures. The origin of the switch from monotonic to non-monotonic behaviour can be explained by the electrochemical mobilities of proton interstitials and electron holes: For high temperatures, electron holes are more mobile than proton interstitials and for low temperatures, the protonic mobility is higher. If the electrochemical mobilities of proton interstitials and electron holes are equal, single-fold conductivity relaxation curves are obtained although a two-fold stoichiometry relaxation may be present. To monitor this behaviour, another sample property that is dependent only on the hydrogen content of the sample must be used.

Conflicts of interest

There are no conflicts to declare.

Appendix A: Diffusion Model

For a plane sheet, the analytical solution to a diffusion model with surface reaction and diffusive flux is described in Reference[6]. The initial concentrations are uniform, $c_i(x,t) = c_i^0$, the gas concentration is constant. Within the bulk phase, Fick's first law describes the flux of charge carriers. The net flux vanishes in the center of the sample due to symmetry, $j_i(t, x = 0) = 0$. At the surface ($x = -a$ and $x = a$), a first order surface reaction takes place. The reactive flux at the surface must be equal to the diffusion flux at the surface,

$$j_i(x = -a) = \tilde{k}_i \left[c_i^{eq} - c_i(x = -a)\right] = -\tilde{D}_i \left.\frac{\partial c_i}{\partial x}\right|_{x=-a} \tag{30}$$

The integrated analytical solution to the diffusion model with two coupled species, e.g. $2j_{v_O^{\bullet\bullet}} = -j_{h^\bullet}$, and their corresponding ambipolar diffusion coefficient $\tilde{D}$ can be expressed by[6,32,38]

$$\frac{\bar{c}_i(t) - c_i^0}{c_i^{eq} - c_i^0} = 1 - \sum_{i=1}^{\infty} \frac{2L_a^2 \cdot \exp\left\{-\beta_i^2 \tilde{D} t a^{-2}\right\}}{\beta_i^2(\beta_i^2 + L_a^2 + L_a)} \tag{31}$$

with the solutions β_i for $L_a = \beta \tan\beta = a\tilde{k}\tilde{D}^{-1}$ and $\bar{c}_i$ as the average concentration over the sample. For a cuboid ingot with dimensions $c \gg a \approx b$ that is used in the experimental setup, an additional summand for the second dimension must be formed.[32–34] For relaxations upon hydration with three mobile charge carriers, however, the diffusion model becomes more complicated (see text).

Appendix B: Diagonalization of Diffusion Coefficients

The matrix of diffusion coefficients described above is a symmetric matrix with real elements only. Here, the principal axis theorem can be used to find the orthogonal (effective) diffusion coefficients, i.e. for the decoupled fluxes. In the first step, the eigenvalue λ must be found which sets the determinant of the flux

matrix zero:

$$\left|\begin{pmatrix} D_{\mathrm{HH}}-\lambda & D_{\mathrm{Hv}} \\ D_{\mathrm{vH}} & D_{\mathrm{vv}}-\lambda \end{pmatrix}\right| = 0 \tag{32}$$

The two solutions for Eq. (32) are

$$\lambda_{1,2} = \frac{D_{\mathrm{HH}}+D_{\mathrm{vv}}}{2} \pm \sqrt{\left(\frac{D_{\mathrm{HH}}+D_{\mathrm{vv}}}{2}\right)^2 - D_{\mathrm{HH}}D_{\mathrm{vv}} + D_{\mathrm{Hv}}D_{\mathrm{vH}}} \tag{33}$$

The two corresponding eigenvectors $\vec{x}_i$ for $\mathbf{D}\vec{x}_i = \lambda_i\vec{x}_i$ with $i = \{1,2\}$ are obtained by solving the linear equations and contain a free parameter as their second element, each. They are normalized to a length of unity with normalization factors m and n, e.g. $\sqrt{(mx_{1(1)})^2+m^2} = 1$ for the first eigenvector, and form an orthogonal matrix $\mathbf{S}$ as column vectors, $\mathbf{S} = [m\vec{x}_1\ n\vec{x}_2]$.

$$\mathbf{S} = \begin{pmatrix} -\frac{D_{\mathrm{Hv}}}{\sqrt{(D_{\mathrm{HH}}-\lambda_1)^2+D_{\mathrm{Hv}}^2}} & -\frac{D_{\mathrm{vv}}-\lambda_2}{\sqrt{D_{\mathrm{vH}}^2+(D_{\mathrm{vv}}-\lambda_2)^2}} \\ \left[1+\left(\frac{D_{\mathrm{Hv}}}{D_{\mathrm{HH}}-\lambda_1}\right)^2\right]^{-1/2} & \left[1+\left(\frac{D_{\mathrm{vv}}-\lambda_2}{D_{\mathrm{vH}}}\right)^2\right]^{-1/2} \end{pmatrix} \tag{34}$$

With the orthogonal matrix $\mathbf{S}$ and its transposed counterpart, $\mathbf{S}^T$, the diffusion matrix $\mathbf{D}$ can be diagonalized, resulting in a new version of Fick's second law, $\mathbf{S}^T\vec{c} = \mathbf{S}^T\mathbf{D}\mathbf{S}(\mathbf{S}^T\vec{c}'')$, where $\mathbf{S}^T\mathbf{D}\mathbf{S}$ is the diagonalized diffusion matrix. A new concentration vector has thus been defined, $\vec{\tilde{c}} = \mathbf{S}^T\vec{c}$, with decoupled concentrations as its elements, $\tilde{c}_i$, where each concentration $\tilde{c}_i$ has a contribution of oxygen vacancies and protons.

References

1 H.-I. Yoo, J.-K. Kim and C.-E. Lee, *J. Electrochem. Soc.*, 2009, **156**, B66–B73.

2 H.-I. Yoo and C.-E. Lee, *Solid State Ionics*, 2009, **180**, 326–337.

3 H.-I. Yoo and C.-E. Lee, *J. Am. Ceram. Soc.*, 2005, **88**, 617–623.

4 D.-K. Lim, H.-N. Im, S.-Y. Jeon, J.-Y. Park and S.-J. Song, *Acta Mater.*, 2013, **61**, 1274–1283.

5 D.-K. Lim, T.-R. Lee, B. Singh, J.-Y. Park and S.-J. Song, *J. Electrochem. Soc.*, 2014, **161**, F710–F716.

6 J. Crank, *The Mathematics of Diffusion*, Oxford University Press, Oxford (UK), second ed. edn, 1975.

7 C. Solís, S. Escolástico, R. Haugsrud and J. M. Serra, *J. Phys. Chem. C*, 2011, **115**, 11124–11131.

8 M. Ruf, C. Solís, S. Escolástico, R. Dittmeyer and J. M. Serra, *J. Mater. Chem. A*, 2014, **2**, 18539–18546.

9 T. Shimura, S. Fujimoto and H. Iwahara, *Solid State Ionics*, 2001, **143**, 117–123.

10 R. Haugsrud and T. Norby, *Nat Mater*, 2006, **5**, 193–196.

11 R. Haugsrud, *Solid State Ionics*, 2007, **178**, 555–560.

12 D. van Holt, E. Forster, M. E. Ivanova, W. A. Meulenberg, M. Müller, S. Baumann and R. Vaßen, *J. Eur. Ceram. Soc.*, 2014, **34**, 2381–2389.

13 E. Forster, D. van Holt, M. E. Ivanova, S. Baumann, W. A. Meulenberg and M. Müller, *J. Eur. Ceram. Soc.*, 2016, **36**, 3457–3464.

14 A. Magrasó, C. Frontera, D. Marrero-López and P. Núñez, *Dalton Trans.*, 2009, 10273.

15 A. Magrasó, J. M. Polfus, C. Frontera, J. Canales-Vázquez, L.-E. Kalland, C. H. Hervoches, S. Erdal, R. Hancke, M. S. Islam, T. Norby and R. Haugsrud, *J. Mater. Chem.*, 2012, **22**, 1762.

16 T. Scherb, S. A. J. Kimber, C. Stephan, P. F. Henry, G. Schumacher, J. Just, S. Escolástico, J. M. Serra, J. Seeger and A. H. Hill, *ArXiv e-prints*, 2013, arXiv:1305.3385v1 [cond–mat.mtrl–sci].

17 A. Magrasó and R. Haugsrud, *J. Mater. Chem. A*, 2014, **2**, 12630–12641.

18 T. Norby, *J. Korean Ceram. Soc.*, 2010, **47**, 19–25.

19 S. Erdal, L.-E. Kalland, R. Hancke, J. M. Polfus, R. Haugsrud, T. Norby and A. Magrasó, *Int. J. Hydrogen Energy*, 2012, **37**, 8051–8055.

20 R. K. Datta and R. Roy, *J. Am. Ceram. Soc.*, 1967, **50**, 578–583.

21 K.-D. Kreuer, *Chem. Mater.*, 1996, **8**, 610–641.

22 K.-D. Kreuer, *Annu. Rev. Mater. Res.*, 2003, **33**, 333–359.

23 M. E. Björketun, P. Sundell, G. Wahnström and D. Engberg, *Solid State Ionics*, 2005, **176**, 3035–3040.

24 J.-S. Choi, D.-K. Lee and H.-I. Yoo, *J. Korean Ceram. Soc.*, 2000, **37**, 271–279.

25 H.-I. Yoo and M. Martin, *Phys. Chem. Chem. Phys.*, 2010, **12**, 14699.

26 E. Kim, J. in Yeon, M. Martin and H.-I. Yoo, *Solid State Ionics*, 2013, **235**, 22–31.

27 D. Poetzsch, R. Merkle and J. Maier, *Adv. Funct. Mater.*, 2015, **25**, 1542–1557.

28 R. Merkle, W. Sitte and J. Maier, *Solid State Ionics*, 2020, **347**, 115174.

29 J. Seeger, M. E. Ivanova, W. A. Meulenberg, D. Sebold, D. Stöver, T. Scherb, G. Schumacher, S. Escolástico, C. Solís and J. M. Serra, *Inorg. Chem.*, 2013, **52**, 10375–10386.

30 W. Deibert, V. Stournari, M. E. Ivanova, S. Escolástico, J. M. Serra, J. Malzbender, T. Beck, L. Singheiser, O. Guillon and W. A. Meulenberg, *J. Eur. Ceram. Soc.*, 2018, **38**, 3527–3538.

31 R. Haugsrud and C. Kjølseth, *J. Phys. Chem. Solids*, 2008, **69**, 1758–1765.

32 H. S. Carslaw and J. C. Jaeger, *Conduction of heat in solids*, Clarendon, Oxford, 2nd edn, 1959.

33 I. Yasuda and M. Hishinuma, *J. Solid State Chem.*, 1996, **123**,

382–390.
34 A. Falkenstein, D. N. Mueller, R. A. De Souza and M. Martin, *Solid State Ionics*, 2015, **280**, 66–73.
35 D. Poetzsch, R. Merkle and J. Maier, *Phys. Chem. Chem. Phys.*, 2014, **16**, 16446–16453.
36 W. Preis and W. Sitte, *Solid State Ionics*, 2016, **288**, 286–290.
37 D. Poetzsch, R. Merkle and J. Maier, *Faraday Discuss.*, 2015, **182**, 129–143.
38 B. Ma, U. Balachandran, J.-H. Park and C. Segre, *Solid State Ionics*, 1996, **83**, 65–71.